Sensors & Diagnostics

PAPER

View Article Online
View Journal | View Issue

Check for updates

Cite this: *Sens. Diagn.*, 2025, **4**, 82

Selection of ssDNA aptamers and construction of an aptameric electrochemical biosensor for detecting *Giardia intestinalis* cyst protein†

Mohammed Alhindawi,[a] Amina Rhouati,[ab] Rahmah Noordin,[c] Dana Cialla-May,[de] Jürgen Popp[de] and Mohammed Zourob[*a]

Giardia intestinalis, an intestinal protozoan parasite, is one of the potentially severe parasitic infections, especially in children. Rapid and simple diagnostic tools are highly desired to prevent the potential outbreak of *G. intestinalis* infection. The life cycle of Giardia species is quite simple and consists of trophozoite and cystic forms. This report presents the selection of ssDNA aptamers with high binding affinity to a *G. intestinalis* cyst recombinant protein using the SELEX process (systematic evolution of ligands by exponential enrichment). The process is based on incubating a random DNA library with the targeted protein, and the bound sequences are recovered and amplified by polymerase chain reaction (PCR). The generated pool of aptamer sequences is used in the subsequent selection round. After ten selection cycles, three sequences were isolated with low dissociation constants (K_d) of 7.98, 21.02, and 21.86 nM. Subsequently, the aptamer with the best affinity was integrated into a label-free electrochemical biosensor to detect *G. intestinalis* cyst protein. The developed aptasensor accurately detected the *G. intestinalis* recombinant cyst protein within the range of 0.1 pg mL^{-1} to 1000 ng mL^{-1}, and a low detection limit of 0.0026 pg mL^{-1}. Furthermore, a selectivity study showed insignificant cross-reactivity against other proteins such as bovine serum albumin and globulin, and no reactivity against *G. intestinalis* trophozoite recombinant protein. Finally, the aptasensor was tested using *G. intestinalis*-spiked tap water samples and showed good recovery rates.

Received 1st September 2024,
Accepted 27th November 2024

DOI: 10.1039/d4sd00296b

rsc.li/sensors

Open Access Article. Published on 12 December 2024. Downloaded on 7/30/2025 11:42:54 AM.
This article is licensed under a Creative Commons Attribution-NonCommercial 3.0 Unported Licence.

Introduction

Infectious diseases caused by protozoan parasites affect millions in underdeveloped and developing countries, leading to worldwide health concerns.[1] The high rate of infection by protozoan parasites is mainly related to poor sanitary conditions or immunodeficiency.[2,3] *Giardia intestinalis* (*G. intestinalis*) is a ubiquitous flagellated protozoan parasite. The Giardia lifecycle has two phases: an active feeding and dividing phase (trophozoite) and an inactive infectious phase (cyst) resistant to environmental conditions.[4] Transmission occurs by ingestion of Giardia cysts in food and water, and on skin and surfaces that have been contaminated with faeces containing the protozoa. Symptomatic giardiasis produces gastrointestinal problems such as diarrhoea, abdominal cramps, greasy stools, bloating, nausea, vomiting, weight loss, and dehydration.[4]

Cysts are found in most natural water sources, such as rivers, lakes, ponds, and streams, but they are more likely to be found in areas contaminated with animal feces.[5,6] Once *G. intestinalis* cysts enter the human body and are exposed to gastric acid, the excystation process starts which breaks down the hardy cyst wall. Then, in the small intestine, each cyst produces two excyzoites, then generates four trophozoites following cell division. Finally, some trophozoites initiate the encystation process and move to the lower intestine, where they are shed from the host's faeces to the outside environment as infective cysts.[7,8] The standard methods used for *G. intestinalis* detection are based on microscopic observation of stained clinical samples, immunological and PCR tests.[9,10] However, microscopic detection lacks from sensitivity, while molecular techniques are expensive and time-consuming.[11]

[a] *Department of Chemistry, Alfaisal University, Al Zahrawi Street, Al Maather, Al Takhassusi Rd, Riyadh 11355, Saudi Arabia. E-mail: mzourob@alfaisal.edu*
[b] *Bioengineering laboratory, Higher national school of Biotechnology, Constantine, Algeria*
[c] *Department of Parasitology and Medical Entomology, Faculty of Medicine, Universiti Kebangsaan Malaysia, 56000 Cheras, Kuala Lumpur, Malaysia*
[d] *Institute of Physical Chemistry (IPC) and Abbe Centre of Photonics (ACP), Friedrich Schiller University Jena, Member of the Leibniz Centre for Photonics in Infection Research (LPI), Helmholtzweg 4, 07743 Jena, Germany*
[e] *Leibniz Institute of Photonic Technology, Member of Leibniz Health Technologies, Member of the Leibniz Centre for Photonics in Infection Research (LPI), Albert-Einstein-Straße 9, 07745 Jena, Germany*

† Electronic supplementary information (ESI) available. See DOI: https://doi.org/10.1039/d4sd00296b

© 2025 The Author(s). Published by the Royal Society of Chemistry

Open Access Article. Published on 12 December 2024. Downloaded on 7/30/2025 11:42:54 AM.
This article is licensed under a Creative Commons Attribution-NonCommercial 3.0 Unported Licence.

Aptamers are short single-stranded oligonucleotides selected to bind various molecules with high affinity and specificity.[12] They are generated by SELEX process (systematic evolution of ligands by exponential enrichment), starting from a pool of 10^{14} to 10^{15} random oligonucleotide sequences. Target-specific candidates are recovered and amplified by polymerase chain reaction (PCR). The obtained pool of sequences is then exposed to iterative selection cycles with gradual increasing degrees of stringency to ensure the successful selection of high affinity binders.[13] Finally, the selected aptamers are cloned and sequenced.[14–16]

Aptasensors, as their name suggests, use an aptamer as the biorecognition element to bind to an analyte, and the biorecognition mechanism is structure or conformational-dependent.[17,18] Aptasensors are promising diagnostic tools that have shown high sensitivity and selectivity, low-cost fabrication, and high stability. Aptamers can be labelled with several types of dyes and modified with different chemical groups. They can be applied in a wide range of optical, and electrochemical biosensing.[19] Electrochemical aptasensors have gained significant attention due to their exceptional sensitivity, selectivity, stability, and rapid response, combining the advantages of electrochemical techniques with the specific recognition ability of aptamers. The principle of detection is based on monitoring the variation of the electrical current resulting from the electrochemical interactions occurring at the electrode surface.[20,21] Electrochemical aptasensors have been applied in different fields including environmental monitoring and biomedical diagnostics.[22] There are several reports on parasite detection using aptasensor. Iqbal *et al.* developed a specific aptasensor to detect *Crptosporidium parvum* oocysts in spiked fresh fruits.[23] In another report, Chakma *et al.* used the SELEX process to develop an ssDNA aptamer against the histine rich protein-II (HRP-II), a specific biomarker for *Plasmodium falciparum.*[24] Young Lo *et al.* also developed an aptamer against *P. falciparum* HRP-II (PfHRP2) and subsequently an electrochemical aptamer-based biosensor to detect malaria.[25] Recently, we applied the SELEX process to generate the first aptamer targeting a *G. intestinalis* trophozoite recombinant protein. Using the aptamer, we developed an electrochemical aptasensor exhibiting high affinity to the target.[26]

Herein, we focus on the selection of a second aptamer recognizing the *G. intestinalis* cyst recombinant protein *via* the SELEX process. After ten rounds, the selected candidate underwent an affinity test. The aptamer exhibiting the lowest dissociation constant was employed in the design of an electrochemical biosensing platform. The detection mode is based on the change of electron transfer resulting from the interaction between the aptamer and the cyst recombinant protein. A wide linear range of detection was achieved with a high sensitivity and selectivity against other potential interfering proteins. Finally, the analytical tests performed on spiked tap water samples demonstrated the applicability of our aptasensor without interfering effects. This work complements our previous study reporting trophozoite aptamer, allowing the discrimination between the two phases of *G. intestinalis* development.

Experimental

1. Materials and reagents

Materials and Chemicals are provided in the ESI.†

2. Instrumentation

The instrumentation is provided in the ESI.†

3. Screening of DNA aptamer specific to a *G. intestinalis* cyst recombinant protein

A random ssDNA library consisting of 1.8×10^{15} oligonucleotides was used for the aptamer selection process. The central sequence of the ssDNA library has 40 nucleotides flanked by two primer annealing sites of 16 nucleotides at the 3′ and 5′ ends. *G. intestinalis* cyst recombinant protein was immobilized on the NHS-sepharose beads. Then, the protein-conjugated beads were incubated with 50 mM Tris buffer (pH 8) for one hour to eliminate the remaining non-specific sites on the beads. The conjugated beads were washed four times using two washing buffers alternately, *i.e.* washing buffer 1 consists of (50 mM sodium acetate, 0.5 M NaCl, pH 4.0–4.5) and washing buffer 2 which contains (50 mM Tris, 0.5 M NaCl pH 8). The washed beads were stored in 10 mM Tris, pH 7.5, containing 0.05% sodium azide, at 4 °C until further use. To confirm the immobilization of the protein on the beads, we measured the protein amount before immobilization and after each washing step. Table S1† shows the measured protein amount for each step. We calculated the immobilized protein amount (1.18 mg) as $P_{im} = P_0\_P_1$, where P_{im} is the immobilized amount, P_0 is the initial amount and P_1 is the amount measured in the washing fractions.

G. intestinalis cyst recombinant protein-conjugated beads (100 μL) were washed five times with 500 μL binding buffer and centrifuged at 1000 × *g* for 5 minutes. The DNA library was then incubated with the recombinant protein-conjugated beads for two hours at room temperature. After washing six times with the binding buffer, the bound sequences were eluted by adding 500 μL boiling water to the filter and incubating for 5 minutes at 90 °C, followed by centrifuging at 50 000 × *g* for one minute. The elution step was repeated five times, and the DNA was collected. The DNA was concentrated by centrifuging at 17 000 × *g* for 1 minute using an ultra-filtration device with a 3 kDa cut-off membrane.

The eluted DNA pools were amplified by PCR. Taq Plus polymerase, buffer, 2 mM $MgCl_2$, 200 μM dNTP, 0.2 μM of forward and reverse primers were used. PCR cycles were run as follows: 94 °C denaturation for 10 min, followed by 25 cycles of 94 °C for 1 min, 47 °C for 1 min, 72 °C for one minute, and a final extension step of 10 minutes at 72 °C. For asymmetric PCR, fluorescein amidites was used to prepare fluorescein-labeled oligonucleotide probes for detecting the

Open Access Article. Published on 12 December 2024. Downloaded on 7/30/2025 11:42:54 AM.
This article is licensed under a Creative Commons Attribution-NonCommercial 3.0 Unported Licence.

complementary nucleic acids or primers for PCR. The collected DNA were quantified by UV-spectrophotometry and used for the subsequent selection cycle.

The DNA obtained from the last round of the SELEX was cloned into the pCR2.1-TOPO vector and transformed into *Escherichia coli* competent cells. Luria-Bertani (LB)-agar plates supplemented with ampicillin, X-Gal (5-bromo-4-chloro-3-indolyl-beta-D-galactoside), and IPTG (isopropyl beta-D-1-thiogalactopyranoside) were used to grow the recombinant *Escherichia coli*. The white (positive) colonies were picked and grown in LB liquid media. Subsequently, the ssDNA inserts (aptamers) were amplified using M13 forward and reverse primer sites within the vector. Finally, the identified aptamers specific to the *G. intestinalis* cyst recombinant protein were sequenced and aligned using the PRALINE software (**https://www.ibi.vu.nl/programs/pralinewww/**).

4. Dissociation constants (K_d) determination

To measure the dissociation constants (K_d) of the selected aptamers, different concentrations of fluorescent dye (FAM)-labelled aptamers were incubated with the target-conjugated beads for one hour. Then, the beads were washed with the binding buffer, and the bound DNA was eluted. The fluorescence intensity of the eluted DNA at each concentration was measured and used to plot the binding curves. The K_d for each *G. intestinalis* cyst protein aptamer was determined by non-linear regression analysis of the binding curve. A saturation curve was plotted for each sequence, and the dissociation constants were calculated by nonlinear regression analysis using Prism Software (**https://www.graphpad.com/features**).

5. Electrochemical aptasensing of *G. intestinalis* cyst protein

The dissociation constants (K_d) of the *G. intestinalis* cyst aptamers were estimated following the procedure described in the previous chapter. The aptamer that showed the highest affinity (cyst 1) to our target was used to develop the electrochemical aptasensor. Cyst 1 aptamer was first conjugated to a thiol group at the 5′ end to enable its assembly onto the screen gold-printed electrodes. The functionalized electrode was then incubated with 6-mercapto-1-hexanol (MCH) to block the non-specific sites. For the electrochemical detection experiments, 10 μL of increasing concentrations of *G. intestinalis* cyst recombinant protein solution (0.1, 1, 10, 10, 100, 1000, 10 000, and 100 000 pg mL^{-1}) prepared in binding buffer were incubated on the aptasensor surface for 30 minutes. Then, the electrodes were washed with 1% phosphate buffered saline (PBS), pH 7.4 to remove the non-specific bound molecules. The electrochemical response was recorded in the presence of $[Fe(CN)6]^{-4/-3}$ redox couple using square wave voltammetry (SWV). Selectivity experiments were conducted by incubating the aptasensor with 100 ng ml^{-1} of bovine serum albumin (BSA), globulin, and *G. intestinalis* trophozoite recombinant protein.

Results and discussion

1. Selection of DNA aptamers for *G. intestinalis* cyst recombinant protein

The SELEX progress was monitored by determining the DNA recovery after each round by measuring the fluorescence intensity of the eluted DNA. Fig. 1 shows the fluorescence intensity of the recovered amount of DNA measured after each round. From cycle 1 to 6, the fluorescence intensity increased, signalling DNA enrichment after each cycle. Then, in a counter selection step, the DNA pool was incubated with negative beads (the non-conjugated beads) to remove the non-specific binding to the NHS-sepharose beads. The collected DNA were washed and incubated with target-conjugated beads, then the same heating and cooling treatment were performed as the normal selection rounds. As shown in Fig. 1, a drop in the fluorescence intensity was recorded in cycle 8, confirming the removal of the non-specific DNA sequences. After counter selection, cycles 9 and 10 showed a significant increase of the fluorescence intensity confirming the enrichment of the specific aptamer candidates for the *G. intestinalis* cyst protein. The constant fluorescence recovery after ten selection rounds indicates the saturation of the specific binding sites and that there are no more sites available for binding.

The obtained sequences were cloned into the pCR2.1-TOPO vector and transformed into *E. coli* competent cells. Twenty-two positive colonies were picked and sequenced, and three aptamer sequences were successfully obtained. The three sequences then underwent binding affinity studies. Finally, the obtained aptamers specific to *G. intestinalis* cyst protein were sequences and aligned *via* PRALINE software.

Secondary structure of the final aptameric ligand was predicted by online server Mfold shown in Fig. S1.† Overall secondary structure of an aptamer is critical for its function, as it directly influences its ability to bind to the target

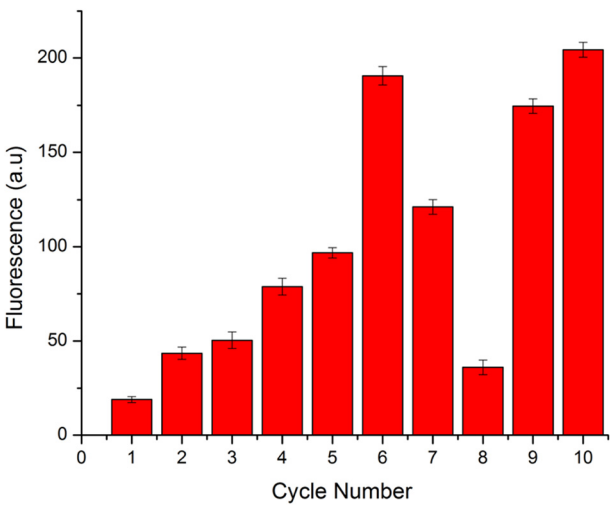

Fig. 1 Fluorescence intensity of the *Giardia intestinalis* cyst recombinant protein-specific aptamers during the SELEX procedure.

© 2025 The Author(s). Published by the Royal Society of Chemistry

Open Access Article. Published on 12 December 2024. Downloaded on 7/30/2025 11:42:54 AM. This article is licensed under a Creative Commons Attribution-NonCommercial 3.0 Unported Licence.

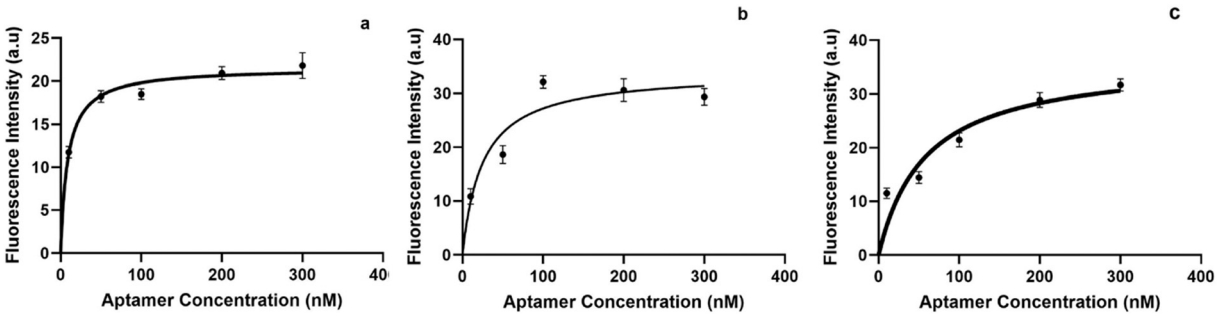

Fig. 2 Saturation binding affinity curves obtained, for the (a) cyst 1, (b) cyst 2 and (c) cyst 3.

Table 1 Sequences and dissociation constants of the selected aptamers

Aptamer	Sequence (5′ → 3′)	K_d (nM)
Cyst 1	5′-TCA GTC ATT ATG TAT GCT TGA TCA CTT ATC CGT CTG CCG T-3′	7.98
Cyst 2	5′-ATC CAC ACG GCG AGC TGT ATT ATT GCC AAC TGA GCA AAT A-3′	21.02
Cyst 3	5′-GTG GAT TGT CGT ACG ACA TAA TAA TTG GAT ATC AGG ACA T-3′	21.86

molecule. The flexibility of aptamers allows them to evolve and adapt to bind their targets. In cyst 1 aptamer, nucleotide 6–16 forms the stem-loop 1 (SL1) region, and nucleotide 20–30 forms the stem-loop 2 (SL2) region. For aptamers that bind proteins, the stem-loop structure can facilitate multiple, cooperative binding interactions, leading to stronger binding (higher affinity). The loop can act as a functional binding site, while the stem region could assist by stabilizing the aptamer-target complex. In addition, The stem-loop structure enables induced-fit mechanisms where the aptamer undergoes a conformational change upon binding, increasing the interaction strength.[27] Moreover, a well-exposed and flexible loop, enhance the aptamer ability to interact with a wider range of amino acid residues on the protein, improving binding strength. On the other hand, the stem part, primarily stabilizing the loop, can also help orient the aptamer correctly for efficient interaction, thus increasing the aptamer-protein binding efficiency.[28]

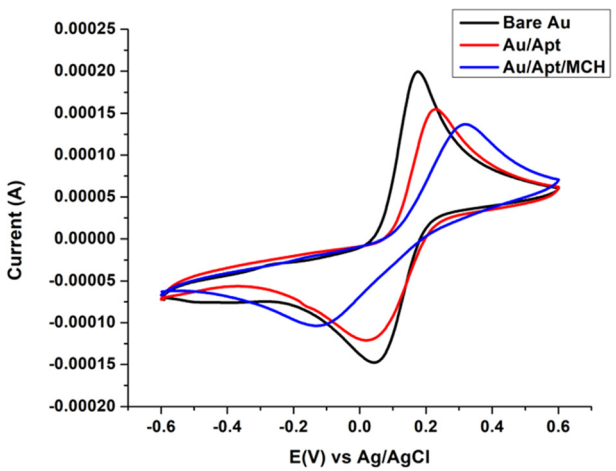

Fig. 3 Cyclic voltammograms obtained in a 5 mM solution of $[Fe(CN)_6]^{4-/3-}$ redox couple in PBS buffer, pH 7.4 (black curve) bare SPGE, (red curve) SPGE functionalized with *G. intestinalis* cyst protein aptamer and (blue curve) SPGE/aptamer after blocking with 6-mercapto-1-hexanol (MCH).

2. Affinity determination of the selected aptamers

The three selected aptamer sequences were labelled with a fluorescent dye: carboxyfluorescein (FAM) to measure the affinity of the selected aptamers. Different concentrations of the aptamers (from 0 to 200 nM) were incubated with a fixed amount of *G. intestinalis* cyst protein-conjugated beads under the same experimental conditions described in part 4 of the experimental section above. The fluorescence measurements were performed after DNA elution to study the binding affinities. The fluorescence intensities were used to plot the binding curve shown in Fig. 2.

Table 1 shows the three selected aptamer sequences, cyst 1, cyst 2, and cyst 3, and their corresponding K_d values (7.98, 21.02 and 21.86 nM). The aptamer exhibiting the lowest K_d (cyst 1) was chosen to perform the subsequent experiments to detect *G. intestinalis* cyst protein.

3. Electrochemical aptasensing of *G. intestinalis* cyst protein

3.1 Characterization of the aptasensor fabrication steps. From the three sequences selected against *G. intestinalis* cyst protein, the aptamer showing the lowest K_d value (cyst 1) was used to construct an electrochemical biosensing platform. The aptamer was first conjugated to a thiol group (Metabion, Germany) to enable its immobilization on the gold surface of the screen-printed electrodes. The covalent binding between the thiolated aptamer and the gold surface led to the formation of a self-assembled monolayer, raising the aptasensor's sensitivity by improving the accessibility of the aptamer-specific sites to the cyst protein binding.[28]

The cyclic voltammetric measurements carried out on the gold electrode in $[Fe(CN)_6]^{3-/4-}$ redox couple solution

Open Access Article. Published on 12 December 2024. Downloaded on 7/30/2025 11:42:54 AM.
This article is licensed under a Creative Commons Attribution-NonCommercial 3.0 Unported Licence.

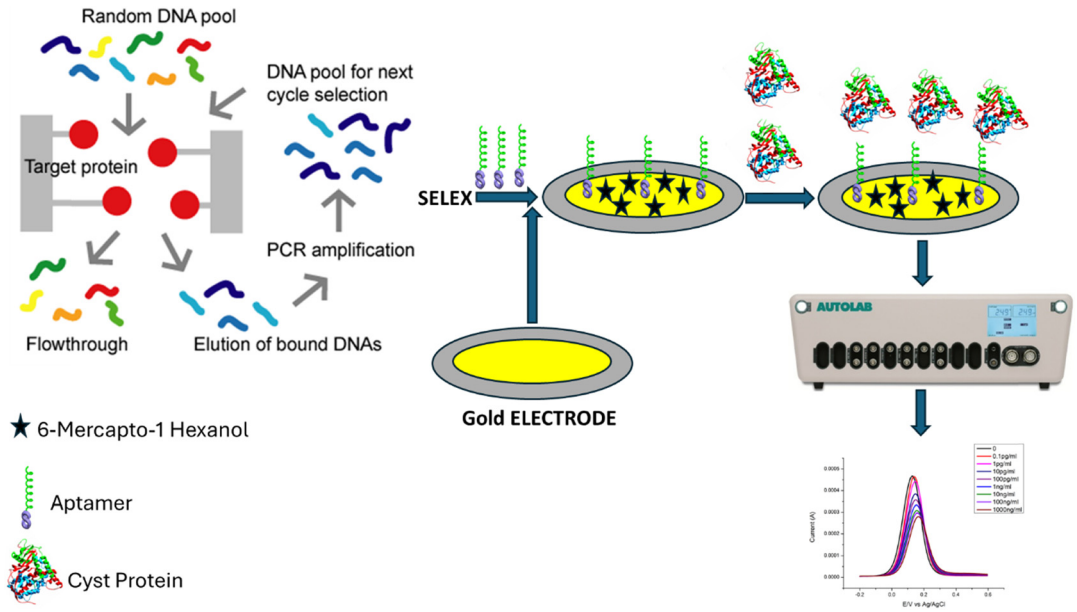

Scheme 1 Aptamer selection and fabrication steps of the *G. intestinalis* cyst protein aptasensor.

prepared in PBS buffer at pH 7.4 are shown in Fig. 3, before and following each modification step. In the black curve with a peak-to-peak separation (ΔE) of around 0.17 V, the bare gold electrode displayed pure gold's distinct reversible CV behavior. It also displayed distinct anodic and cathodic peaks. The cyst recombinant protein aptamer then displayed a drop in the peak current and increased in the ΔE to 0.20 V, as shown in the red curve. The phenomenon can be explained by the negative charges of the ssDNA backbone, which acts as a barrier hampering the transfer of electrons to the surface. The decrease in current peaks confirmed the covalent attachment of aptamer molecules to the gold surface. Mercaptohexanol (MCH) was then added to displace the non-specifically adsorbed portions of the aptamers and guaranteed their vertical orientation, due to the repulsion between the negative alcohol terminus and the negatively charged DNA backbone. The significant decrease in peak currents and the ΔE increased to 0.24, shown in the blue curve, demonstrating the effective blocking step.

3.2 Electrochemical aptasensing of *G. intestinalis* cyst recombinant protein. To study the applicability of the generated aptamer in detecting *G. intestinalis* cyst recombinant protein, an aptasensing platform was developed by immobilizing the selected aptamer on screen-printed gold electrode. The fabrication steps and principle of detection are shown in Scheme 1. A volume of 10 μL droplet of increasing concentrations of *G. intestinalis* cyst recombinant protein solution (0.1, 1.0, 10, 100, 100, 1000, 10 000, and 100 000 pg ml^{-1}) prepared in binding buffer were incubated onto the aptasensor surface for 30 minutes. After incubation, the electrodes were washed with PBS to remove the non-specifically bound molecules, and then the electrochemical measurements were recorded by square wave voltammetry in the presence of the redox couple $[Fe(CN)_6]^{4-/3-}$ with a concentration of 5 mM prepared in PBS buffer, and at a pH value of 7.4. The voltammograms were recorded from −0.2 V to 0.6 V, applying an amplitude of 20 mV; step potential −5 mV; interval time 0.04 s; scan rate 125 mV s^{-1}, and frequency 25 Hz.

Fig. 4a shows the electrochemical responses of the aptasensor before and after binding with different concentrations of the cyst recombinant protein. We observed that the peak current decreased by increasing the *G. intestinalis* cyst protein concentration. This is due to the formation of the complex aptamer target. Our target is a cyst wall protein expressed and purified from the recombinant yeast, *Pichia pastoris*, and its bulky size can inhibit the electron transfer to the surface, resulting in a lower peak. The calibration curve shown in Fig. 4b was plotted using the electrochemical response recorded for each concentration. The response was calculated as $((i^0 - i)/i^0)$ % where i^0 and i correspond to the values of the current peaks before and after the cyst recombinant protein binding, respectively. Fig. 4b showed good linearity obtained in the range of 0.1 pg mL^{-1} to 1 000 000 pg mL^{-1}, with R^2 of 0.96002. The linear regression equation was determined as $((i^0 - i)/i^0)$ % = 13.24 + 11.47 log cyst recombinant protein concentration in (pg mL^{-1}). A detection limit of 0.0026 pg mL^{-1} was calculated as $3\sigma/b$ where σ is the standard deviation of the blank signal and b is the slope of the calibration curve. The calculated detection limit shows a high sensitivity of the proposed aptasensor for *G. intestinalis* cyst protein detection. This high sensitivity could be attributed to the self-assembled monolayer formed between the thiol group and the gold surface, providing a uniform and well oriented bioreceptors.[29] All the measurements were done in triplicates, and the error bars represent the standard deviations of the three trials, demonstrating the high accuracy of the aptasensor.

© 2025 The Author(s). Published by the Royal Society of Chemistry

Open Access Article. Published on 12 December 2024. Downloaded on 7/30/2025 11:42:54 AM.
This article is licensed under a Creative Commons Attribution-NonCommercial 3.0 Unported Licence.

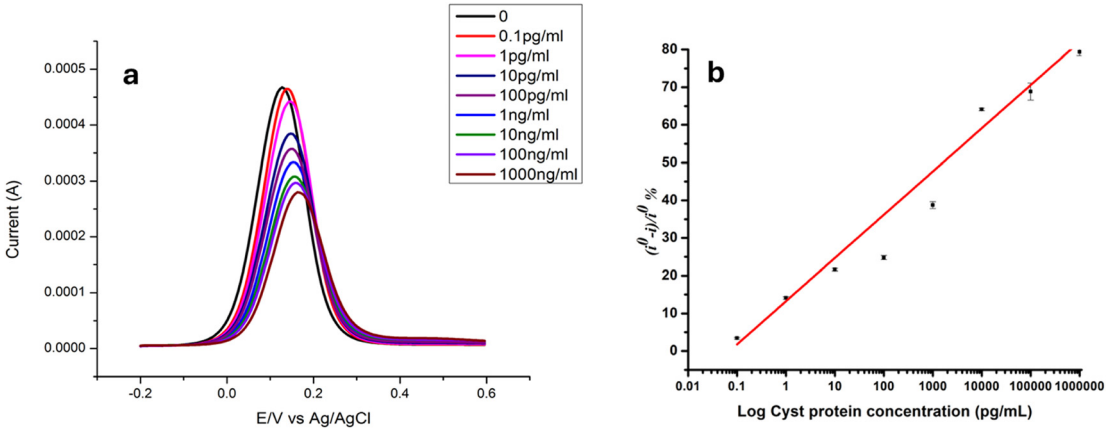

Fig. 4 Square wave voltammograms of the *G. intestinalis* cyst protein aptasensor before and after binding with different concentrations of the *G. intestinalis* cyst protein aptamer ranging from 0.1 to 1 000 000 pg mL^{-1}. The voltammograms were recorded from −0.2 V to 0.6 V, applying an amplitude of 20 mV; step potential −5 mV; interval time 0.04 s; scan rate 125 mV s^{-1}, and frequency 25 Hz (a) and the calibration curve for *G. intestinalis* cyst protein aptasensing. Plot of analytical response ($(i^0 - i)/i^0$%) *versus* logarithm of the cyst recombinant protein concentration. The error bars represent the standard deviations of three repetitive measurements (b).

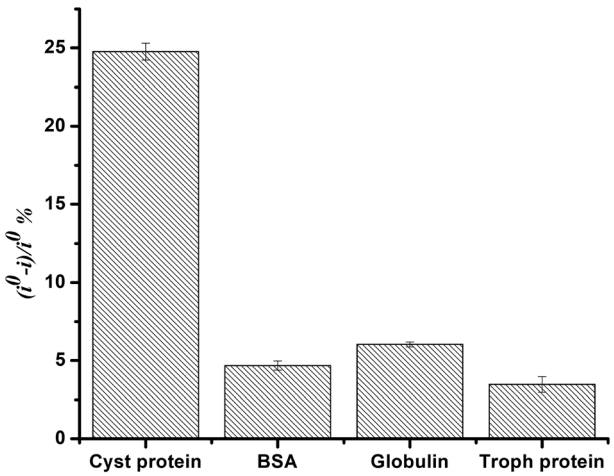

Fig. 5 Comparison of the aptasensor response towards 100 pg mL^{-1} of *G. intestinalis* cyst protein, BSA, globulin, and *G. intestinalis* trophozoite protein.

3.3 Cross reactivity studies. The selectivity of the sensing system of the aptasensor for *G. intestinalis* cyst protein was evaluated by performing a cross-reactivity study. The SPGEs functionalized with the selected cyst 1 aptamer were tested with potential interfering proteins. Different electrodes were separately incubated with a fixed concentration (100 pg mL^{-1}) of Cyst protein, BSA, globulin and *G. intestinalis* trophozoite recombinant protein. Then, detection measurements were performed by SWV using the same conditions described above. The aptasensors responses were calculated as $((i^0 - i)/i^0\%)$ and used to create the histogram bars shown in Fig. 5. It can be shown that the aptasensor response was specific to its target. The response to the cyst protein was six folds higher than to BSA and three folds more than globulin. In addition, a negligible response was obtained with *G. intestinalis* trophozoite recombinant protein, showing the absence of binding between the aptasensor and the trophozoite protein. These results indicate the negligible or no cross-reactivity of the developed aptasensor with the potential interfering proteins and confirm its selectivity for *G. intestinalis* cyst protein This important result can help to increase the targets were chosen to detect, quantify or identify of *G. intestinalis* in water samples.

3.4 Real sample applicability. To test the feasibility of applying the developed aptasensor for the detection of *G. intestinalis* in tap water samples. The samples were first diluted in binding buffer with a ratio of 1 : 1. They were subsequently spiked with two concentrations of *G. intestinalis* recombinant protein within the analytical range (0.1 and 1 pg mL^{-1}). Each sample was incubated with the developed aptasensor in the optimized experimental conditions, separately. The square wave voltammograms were recorded using the same parameters described above. The obtained peak currents were used to calculate the response $((i^0 - i)/i^0)$ % and compare the aptasensor performance in binding buffer and spiked samples. For the tested concentration 0.1 and 1 pg mL^{-1}, the recovery percentages were 88.88% and 116%. These results are in the range 85–110% with RSDs lower than 5% showing the negligible matrix effect on the aptasensor response signal. The recovery percentages/rates

Table 2 Application of the *G. intestinalis* of cyst protein aptasensor in water samples spiked with the recombinant protein (n = 3)

Spiked concentration pg mL^{-1}	Amount found pg mL^{-1}	Recovery%	RSD%
0.1	0.09	88.88	4.2
1	1.19	116	4.1

Open Access Article. Published on 12 December 2024. Downloaded on 7/30/2025 11:42:54 AM.
This article is licensed under a Creative Commons Attribution-NonCommercial 3.0 Unported Licence.

are shown in Table 2 and they confirm the good applicability of the selected aptamer and the developed biosensor.

Conclusion

We presented the first selection and characterization of DNA aptamer sequences for *G. intestinalis* cyst protein. Ten rounds of SELEX were performed that resulted in selection of three aptamers showing high affinity for the cyst protein with dissociation constants in the nanomolar range. The cyst 1 aptamer, which exhibited the highest affinity for the trophozoite protein (K_d = 7.98 nM), was applied in an electrochemical label-free biosensor. The aptasensor detected *G. intestinalis* cyst recombinant protein in the wide linear range of 0.1 pg mL^{-1} to 1000 ng mL^{-1}, with a low detection limit of 0.41 pg mL^{-1}. Moreover, the developed aptasensor was highly selective to the cyst recombinant protein, showing a negligible cross-reactivity to BSA and globulin and no reactivity to *G. intestinalis* trophozoite recombinant protein. The aptasensor was successfully used to detect *G. intestinalis* cyst protein in spiked tap water samples with a high rate of recovery.

Future studies to validate the aptasensor using clinical and environmental samples are needed, including testing more types of samples to confirm its specificity. The Giardia cyst aptasensor has potential applications in preventing giardiasis outbreaks by detecting contamination of *G. intestinalis* cysts in water sources used for drinking, farming, and recreation. It can also be combined in one chip with our previous Giardia trophozoite aptasensor to diagnose human giardiasis.

Data availability

The data that support the findings of this study are available from the corresponding author upon reasonable request.

Conflicts of interest

There are no conflicts to declare.

Acknowledgements

The authors would like to acknowledge the generous funding from the research and graduate office at Alfaisal University.

References

1 S. M. Fletcher, D. Stark, J. Harkness and J. Ellis, Enteric protozoa in the developed world: a public health perspective, *Clin. Microbiol. Rev.*, 2012, **25**(3), 420–449.
2 B. Dixon, L. Parrington, A. Cook, K. Pintar, F. Pollari, D. Kelton and J. Farber, The potential for zoonotic transmission of Giardia duodenalis and Cryptosporidium spp. from beef and dairy cattle in Ontario, Canada, *Vet. Parasitol.*, 2011, **175**(1–2), 20–26.
3 R. Thompson, A. Lymbery and A. Smith, Parasites, emerging disease and wildlife conservation, *Int. J. Parasitol.*, 2010, **40**(10), 1163–1170.
4 T. B. Gardner and D. R. Hill, Treatment of giardiasis, *Clin. Microbiol. Rev.*, 2001, **14**(1), 114–128.
5 R. D. Adam, Biology of Giardia lamblia, *Clin. Microbiol. Rev.*, 2001, **14**(3), 447–475.
6 D. Fraser, N. Bilenko, R. J. Deckelbaum, R. Dagan, J. El-On and L. Naggan, Giardia lamblia carriage in Israeli Bedouin infants: risk factors and consequences, *Clin. Infect. Dis.*, 2000, **30**(3), 419–424.
7 R. E. Brodsky, H. C. Spencer and M. G. Schultz, Giardiasis in American travelers to the Soviet Union, *J. Infect. Dis.*, 1974, **130**(3), 319–323.
8 Y. R. Ortega and R. D. Adam, Giardia: overview and update, *Clin. Infect. Dis.*, 1997, **25**, 545–550.
9 G. Faubert, Immune response to Giardia duodenalis, *Clin. Microbiol. Rev.*, 2000, **13**(1), 35–54.
10 L. S. Garcia, M. Arrowood, E. Kokoskin, G. P. Paltridge, D. R. Pillai, G. W. Procop, N. Ryan, R. Y. Shimizu and G. Visvesvara, Practical guidance for clinical microbiology laboratories: laboratory diagnosis of parasites from the gastrointestinal tract, *Clin. Microbiol. Rev.*, 2018, **31**(1), DOI: **10.1128/cmr.00025-17**.
11 S. Paulos, J. M. Saugar, A. de Lucio, I. Fuentes, M. Mateo and D. Carmena, Comparative performance evaluation of four commercial multiplex real-time PCR assays for the detection of the diarrhoea-causing protozoa Cryptosporidium hominis/parvum, Giardia duodenalis and Entamoeba histolytica, *PLoS One*, 2019, **14**(4), e0215068.
12 M. Jangra, U. Dutta, J. Shah, B. Thapa, R. Nada, N. Gupta, R. Sehgal, V. Sharma and S. Khurana, Role of polymerase chain reaction in stool and duodenal biopsy for diagnosis of giardiasis in patients with persistent/chronic diarrhea, *Dig. Dis. Sci.*, 2020, **65**, 2345–2353.
13 T. K. Sharma and R. Shukla, Nucleic acid aptamers as an emerging diagnostic tool for animal pathogens, *Adv. Anim. Vet. Sci.*, 2014, **2**(1), 50–55.
14 R. Stoltenburg, C. Reinemann and B. Strehlitz, SELEX—A(r) evolutionary method to generate high-affinity nucleic acid ligands, *Biomol. Eng.*, 2007, **24**(4), 381–403.
15 A. D. Ellington and J. W. Szostak, In vitro selection of RNA molecules that bind specific ligands, *Nature*, 1990, **346**(6287), 818–822.
16 M. Mascini, I. Palchetti and S. Tombelli, Nucleic acid and peptide aptamers: fundamentals and bioanalytical aspects, *Angew. Chem., Int. Ed.*, 2012, **51**(6), 1316–1332.
17 B. Sequeira-Antunes and H. A. Ferreira, Nucleic acid aptamer-based biosensors: a review, *Biomedicines*, 2023, **11**(12), 3201.
18 L. F. Yang, M. Ling, N. Kacherovsky and S. H. Pun, Aptamers 101: aptamer discovery and in vitro applications in biosensors and separations, *Chem. Sci.*, 2023, **14**(19), 4961–4978.
19 M. Xie, F. Zhao, Y. Zhang, Y. Xiong and S. Han, Recent advances in aptamer-based optical and electrochemical biosensors for detection of pesticides and veterinary drugs, *Food Control*, 2022, **131**, 108399.

© 2025 The Author(s). Published by the Royal Society of Chemistry

Open Access Article. Published on 12 December 2024. Downloaded on 7/30/2025 11:42:54 AM.
This article is licensed under a Creative Commons Attribution-NonCommercial 3.0 Unported Licence.

20 A. Villalonga, B. Mayol, R. Villalonga and D. Vilela, Electrochemical aptasensors for clinical diagnosis. A review of the last five years, *Sens. Actuators, B*, 2022, **369**, 132318.
21 M. Majdinasab and J. L. Marty, Recent advances in electrochemical aptasensors for detection of biomarkers, *Pharmaceuticals*, 2022, **15**(8), 995.
22 Z. Li, M. A. Mohamed, A. Vinu Mohan, Z. Zhu, V. Sharma, G. K. Mishra and R. K. Mishra, Application of electrochemical aptasensors toward clinical diagnostics, food, and environmental monitoring, *Sensors*, 2019, **19**(24), 5435.
23 A. Iqbal, J. Liu, B. Dixon, B. Zargar and S. A. Sattar, Development and application of DNA-aptamer-coupled magnetic beads and aptasensors for the detection of Cryptosporidium parvum oocysts in drinking and recreational water resources, *Can. J. Microbiol.*, 2019, **65**(11), 851–857.
24 B. Chakma, P. Jain, N. K. Singh and P. Goswami, Development of Electrochemical Impedance Spectroscopy Based Malaria Aptasensor Using HRP-II as Target Biomarker, *Electroanalysis*, 2018, **30**(8), 1847–1854.
25 Y. Lo, Y.-W. Cheung, L. Wang, M. Lee, G. Figueroa-Miranda, S. Liang, D. Mayer and J. A. Tanner, An electrochemical aptamer-based biosensor targeting Plasmodium falciparum histidine-rich protein II for malaria diagnosis, *Biosens. Bioelectron.*, 2021, **192**, 113472.
26 M. Alhindawi, A. Rhouati, R. Noordin, D. Cialla-May, J. Popp and M. Zourob, Selection of ssDNA aptamers and construction of aptameric electrochemical biosensor for the detection of Giardia intestinalis trophozoite protein, *Int. J. Biol. Macromol.*, 2024, **267**, 131509.
27 R. E. Armstrong and G. F. Strouse, Rationally manipulating aptamer binding affinities in a stem-loop molecular beacon, *Bioconjugate Chem.*, 2014, **25**(10), 1769–1776.
28 A. Brown, J. Brill, R. Amini, C. Nurmi and Y. Li, Development of better aptamers: structured library approaches, selection methods, and chemical modifications, *Angew. Chem., Int. Ed.*, 2024, **63**(16), e202318665.
29 F. V. Oberhaus, D. Frense and D. Beckmann, Immobilization techniques for aptamers on gold electrodes for the electrochemical detection of proteins: a review, *Biosensors*, 2020, **10**(5), 45.

© 2025 The Author(s). Published by the Royal Society of Chemistry